Active RIS-Assisted Secure Transmission for Cognitive Satellite Terrestrial Networks

Hehao Niu, Zhi Lin, Kang An, Xiaohu Liang, Yihua Hu,
Dong Li, *Senior Member, IEEE*, and Gan Zheng, *Fellow, IEEE*

***Abstract*—This correspondence develops a physical-layer security scheme for a cognitive-satellite terrestrial network, where the satellite and base station (BS) share the spectrum resource, and multiple eavesdroppers attempt to intercept the private signal from the BS to the mobile user. Different from the commonly used passive reconfigurable intelligent surface (RIS), the active RIS, whose reflecting elements can control both the amplitude and phase of the incident signal, is deployed to cooperatively enhance the secure transmission from the BS to the mobile user, and suppress the interference imposed to the earth station. We attempt to maximize the achievable secrecy rate subject to the transmit power constraint and the interference threshold. To address the above non-convex problem, we propose an effective alternating optimization scheme to jointly optimize the beamformer and artificial noise at the BS, and the reflecting coefficient at the RIS. Simulation results indicate that the impact of the "double fading" can be effectively relieved by using active RIS, thus leading to an apparently enhanced secrecy performance gain compared to those with the passive RIS and no RIS designs.**

***Index Terms*—Cognitive-satellite terrestrial network, active RIS, secure beamforming**

I. Introduction

Cognitive satellite-terrestrial network (CSTN), which shares frequency resources among satellite and terrestrial subnetworks, has been seen as a promising technique to achieve reliable communication in densely and sparsely populated areas [1]. However, due to the broadcasting property of wireless channels, CSTN is vulnerable to security threats [2]. To handle this challenge, the physical layer security (PLS) technique, which uses the random characteristics of wireless channels and signal processing methods to realize communication security, has aroused attention in CSTN [**?**]–[6].

Recently, the advanced technique of reconfigurable intelligent surface (RIS) has been developed to configure the wireless channels to improve the link quality. Specifically, RIS consists of many low cost reflecting elements, whose reflecting properties are controlled by controller a [7]. Thus, by smartly altering the amplitude and phase of the incident signals, RIS can enhance/weaken the signal power at the intended users/unintended users, which has attracted research interest in secure communication [8]–[10].

Meanwhile, researchers have proposed to integrate RIS into CSTN. To be specific, [11] deployed RIS in CSTN to improve the spectral efficiency. Then, [12] proposed a joint transmit and reflecting beamforming (BF) design in a RIS-assisted CSTN to minimize the power consumption. Also, [13] proposed a joint BF design in a RIS-enabled hybrid satellite and near-space communication network. Moreover, [14] studied the joint BF design in refracting RIS empowered hybrid satellite-terrestrial networks. Then, [15] proposed a RIS-assisted transmission strategy for CSTN to improve the security.

Note that the above works assumed that RISs are equipped with pure passive elements, whose performance would be much degraded due to the double-fading attenuation, because the reflected signals need to go through the cascaded channel [16]. To confront this effect, [17] proposed a novel active RIS architecture in which each reflection element is equipped with active load impedances to amplify the incident signal. Then, [18] compared the energy efficiency of active RIS with passive RIS, where the results demonstrated that active RIS outperforms passive RIS. Also, [19] studied whether the active RIS is superior to passive RIS under the same power budget. Recently, [20] studied the active RIS-aided secure transmission and the results revealed the superiority of active RIS in terms of secrecy rate. However, the design and optimization of active RIS-assisted secure CSTN has not been studied yet.

Inspired by these observations, in this work, we study the secure transmission in CSTN with the aid of active RIS, where the satellite serves an earth station (ES) and the base station (BS) communicates with a mobile user (MU) in the presence of several eavesdroppers (Eves). Particularly, we attempt to maximize the secrecy rate by joint optimizing the transmit BF, the artificial noise (AN) and the reflecting coefficient (RC). Since an active RIS amplifies the incident signal and introduces additive noise, the signal model is quite different with the passive RIS-assisted scenario. Besides, the formulated design is difficult to handle due to the non-concave secrecy rate expression. Moreover, the newly introduced amplification factors of the RIS are highly coupled with other variables, thus

This work was supported in part by the National Natural Science Foundation of China (61901490, 61901502, 61901516, 62071352, 62201592) in part by the Research Plan Project of NUDT (ZK21-33), in part by the Young Elite Scientist Sponsorship Program of CAST (2021-JCJQ-QT-048), in part by the National Postdoctoral Program for Innovative Talents (BX20200101), in part by the Macau Young Scholars Program (AM2022011), and in part by the Science and Technology Development Fund, Macau SAR (0018/2019/AMJ, 0110/2020/A3, 0029/2021/AGJ). *(Corresponding author: Zhi Lin.)*

Hehao Niu and Kang An are with the Sixty-third Research Institute, National University of Defense Technology, Nanjing 210007, China (e-mail: niuhaonupt@foxmail.com; ankang89@nudt.edu.cn).

Zhi Lin and Yihua Hu are with the College of Electronic Engineering, National University of Defense Technology, Hefei, 230037, China; Zhi Lin is also with the School of Computer Science and Engineering, Macau University of Science and Technology, Taipa, Macau 999078, China (e-mail: linzhi945@163.com; skl_hyh@163.com).

Xiaohu Liang is with the School of Communications Engineering, Army Engineering University, Nanjing, 210000, China, and also with the School of Information Science and Engineering, Southeast University, Nanjing, 210000, China (e-mail: liangxiaohu688@163.com).

Dong Li is with the School of Computer Science and Engineering, Macau University of Science and Technology, Taipa, Macau, China (e-mail: dli@must.edu.mo).

Gan Zheng is with the Wolfson School of Mechanical, Electrical, and Manufacturing Engineering, Loughborough University, Loughborough LE11 3TU, U.K. (e-mail: g.zheng@lboro.ac.uk).

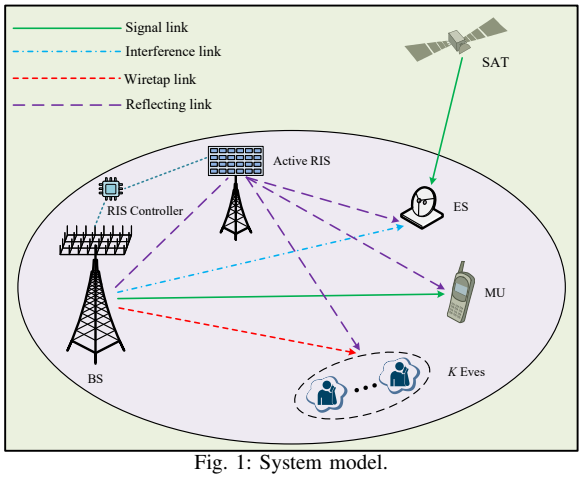

Fig. 1: System model.

making the optimization problem harder to tackle. To address these challenges, we approximate the secrecy rate to a linear function. Then, an alternating optimization (AO) algorithm is developed to optimize these variables iteratively, where each subproblem is a quadratically constrained quadratic program (QCQP). Finally, simulation results confirm the superiority of active RIS in enhancing the security when comparing to other baselines. In addition, we conclude with the following insights: 1) RIS plays a more dominating role than AN in improving the security; 2) The performance advantages of active RIS to passive RIS is more obvious in the low transmit power region of the BS; 3) It is very important to utilize active RIS with properly optimized RC, since the random RC cannot improve the secrecy performance.

Notations: Throughout this paper, the superscript T, $*$ and H denote the transpose, the conjugate, and the conjugate transpose, respectively. $\|\cdot\|$ represents the Frobenius or Euclidean norm. $\mathrm{Diag}\left(a_1,\ldots,a_N\right)$ means a diagonal matrix with $a_1,\ldots,a_N$ on the main diagonal, $\mathrm{diag}\left(\mathbf{A}\right)$ means to extract the main diagonal element of $\mathbf{A}$. $\Re\{\cdot\}$ and $|\cdot|$ denote the real part and modulus. Besides, $\mathcal{CN}\left(\mathbf{x},\mathbf{\Sigma}\right)$ denotes a circularly symmetric complex Gaussian (CSCG) random vector with mean $\mathbf{x}$ and covariance $\mathbf{\Sigma}$, and $\circ$ means the element-wise product. Besides, $\mathrm{Tr}\left(\cdot\right)$ denotes the trace of a matrix.

II. System Model and Problem Formulation

Here, the signal model for the active RIS-assisted CSTN is firstly introduced. Then, we formulate the secrecy rate optimization objective.

A. System Model

We investigate a CSTN as shown in Fig. 1, where a geostationary orbit satellite (GEO) and terrestrial network share the same frequency band. The GEO communicates with an ES, while the BS serves a MU under the eavesdropping of Eves. In addition, a RIS controller is used to configure the RIS. The BS has N antennas and the RIS has M reflecting elements, while the other terrestrial nodes are equipped with a single antenna. We denote $\mathbf{F}\in\mathbb{C}^{M\times N}$ as the channel between the BS and the RIS, $\left\{\mathbf{g}_s^H,\mathbf{g}_u^H,\mathbf{g}_k^H\right\}\in\mathbb{C}^{N\times 1}$, $\left\{\mathbf{h}_s^H,\mathbf{h}_u^H,\mathbf{h}_k^H\right\}\in\mathbb{C}^{M\times 1}$, as the channel from BS/RIS to the ES, MU, and the k-th Eve, respectively.[1]

The BS utilizes a BF $\mathbf{w}\in\mathbb{C}^{N\times 1}$ to send the private signal s satisfying $\mathbb{E}\left\{|s|^2\right\}=1$ to the MU. Meanwhile, the BS sends AN $\mathbf{v}\in\mathbb{C}^{N\times 1}$ to interfere with the Eves. Since the antenna gain of the MU/Eves is much weaker than that of the ES [6], the interference from the satellite to the MU/Eves is omitted. Thus, the received signal at the ES, the MU and the k-th Eve is given as

$$y_s=\left(\mathbf{g}_s^H+\mathbf{h}_s^H\mathbf{\Phi}\mathbf{F}\right)\left(\mathbf{w}s+\mathbf{v}\right)+\mathbf{h}_s^H\mathbf{\Phi}\mathbf{n}_r+n_s, \tag{1a}$$

$$y_u=\left(\mathbf{g}_u^H+\mathbf{h}_u^H\mathbf{\Phi}\mathbf{F}\right)\left(\mathbf{w}s+\mathbf{v}\right)+\mathbf{h}_u^H\mathbf{\Phi}\mathbf{n}_r+n_u, \tag{1b}$$

$$y_k=\left(\mathbf{g}_k^H+\mathbf{h}_k^H\mathbf{\Phi}\mathbf{F}\right)\left(\mathbf{w}s+\mathbf{v}\right)+\mathbf{h}_k^H\mathbf{\Phi}\mathbf{n}_r+n_k, \tag{1c}$$

where $\mathbf{\Phi}=\mathrm{Diag}\left(\phi_1,\ldots,\phi_M\right)\in\mathbb{C}^{M\times M}$ denoting the RC matrix of the RIS, with $\phi_m=\alpha_m e^{j\theta_m}$ being the RC of the m-th element. Here, $\alpha_m\in[0,\alpha_{m,\max}]$ and $\theta_m\in[0,2\pi)$ represent the amplitude and the phase, respectively. For an active RIS, $\alpha_{m,\max}$ is not necessary to be 1. In addition, $\mathbf{n}_r\sim\mathcal{CN}\left(\mathbf{0},\sigma_r^2\mathbf{I}\right)$, $n_s\sim\mathcal{CN}\left(0,\sigma_s^2\right)$, $n_u\sim\mathcal{CN}\left(0,\sigma_u^2\right)$, and $n_k\sim\mathcal{CN}\left(0,\sigma_k^2\right)$ denote noise at the RIS, the ES, the MU, and the k-th Eve, respectively.

Hence, the output signal-to-interference-plus-noise ratio (SINR) at the MU and the k-th Eve is given as

$$\Gamma_u=\frac{\left|\left(\bar{\mathbf{g}}_u^H+\bar{\mathbf{h}}_u^H\mathbf{\Phi}\mathbf{F}\right)\mathbf{w}\right|^2}{\left|\left(\bar{\mathbf{g}}_u^H+\bar{\mathbf{h}}_u^H\mathbf{\Phi}\mathbf{F}\right)\mathbf{v}\right|^2+\sigma_r^2\left\|\bar{\mathbf{h}}_u^H\mathbf{\Phi}\right\|^2+1}, \tag{2a}$$

$$\Gamma_k=\frac{\left|\left(\bar{\mathbf{g}}_k^H+\bar{\mathbf{h}}_k^H\mathbf{\Phi}\mathbf{F}\right)\mathbf{w}\right|^2}{\left|\left(\bar{\mathbf{g}}_k^H+\bar{\mathbf{h}}_k^H\mathbf{\Phi}\mathbf{F}\right)\mathbf{v}\right|^2+\sigma_r^2\left\|\bar{\mathbf{h}}_k^H\mathbf{\Phi}\right\|^2+1}, \tag{2b}$$

where $\bar{\mathbf{g}}_u^H=\mathbf{g}_u^H/\sigma_u$, $\bar{\mathbf{h}}_u^H=\mathbf{h}_u^H/\sigma_u$, $\bar{\mathbf{g}}_k^H=\mathbf{g}_k^H/\sigma_k$, and $\bar{\mathbf{h}}_k^H=\mathbf{h}_k^H/\sigma_k$, respectively. Accordingly, the achievable rates for the MU and the k-Eve are respectively, given by $R_u=\log_2\left(1+\Gamma_u\right)$ and $R_k=\log_2\left(1+\Gamma_k\right)$.

B. Problem Formulation

In this work, we aim to maximize the secrecy rate via joint optimizing the BF $\mathbf{w}$, the AN $\mathbf{v}$, and the RC matrix $\mathbf{\Phi}$. The problem is given as

$$\max_{\mathbf{w},\mathbf{v},\mathbf{\Phi}} F\left(\mathbf{w},\mathbf{v},\mathbf{\Phi}\right)\triangleq\min_k R_u-R_k \tag{3a}$$

$$\text{s.t. } \|\mathbf{w}\|^2+\|\mathbf{v}\|^2\le P_s, \tag{3b}$$

$$\|\mathbf{\Phi}\mathbf{F}\mathbf{w}\|^2+\|\mathbf{\Phi}\mathbf{F}\mathbf{v}\|^2+\sigma_r^2\|\mathbf{\Phi}\|^2\le P_r, \tag{3c}$$

$$\left|[\mathbf{\Phi}]_m\right|\le\alpha_{m,\max},\forall m, \tag{3d}$$

$$\left|\tilde{\mathbf{g}}_s^H\mathbf{w}\right|^2+\left|\tilde{\mathbf{g}}_s^H\mathbf{v}\right|^2+\sigma_r^2\left\|\mathbf{h}_s^H\mathbf{\Phi}\right\|^2\le I_{th}, \tag{3e}$$

with P_s and P_r being the maximum transmit powers at the BS and RIS, respectively. In addition, I_{th} denotes the interference threshold for the ES with $\tilde{\mathbf{g}}_s^H=\mathbf{g}_s^H+\mathbf{h}_s^H\mathbf{\Phi}\mathbf{F}$ being the equivalent channel from BS to ES.

[1]Here, we assume that due to the position of the GEO satellite and the RIS, the signal from the GEO satellite only arrive at the back panel of the RIS and will not be reflected by the RIS. Besides, we assume that the wireless channels undergo slow fading. The angles of arrival (AoA)-based CSI of the MU/Eves are available at BS through cell positioning or satellite GPS and feedback/training sent from the users via a backhaul channel, and this kind of mechanism has already been verified in [24]. Besides, several channel estimation techniques have been investigated to obtain the CSI of the RIS-related links, such as the Hadamard-matrix truncation method in [25], the progressive refinement method in [26], and the parallel factor decomposition method in [27], which makes the acquirement of the CSI become practical.

III. The Joint Design Algorithm

Since the secrecy rate is the difference of two logarithmic functions, (3) is non-convex. To solve (3), we first develop an effective lower bound of the secrecy rate around the given point $\{\mathbf{w}^t, \mathbf{v}^t, \mathbf{\Phi}^t\}$ with t being the iteration time. Then, we propose an AO method to obtain these variables iteratively.

A. An Approximation of the Secrecy Rate

First, we find the following lemma is useful to recast the secrecy rate into a solvable formulation.

Lemma 1 [10]: For any u and ν, we have

$$\log_2\left(1+|\mu|^2\right) \geq \log_2\left(1+|\bar{\mu}|^2\right) - \frac{|\bar{\mu}|^2}{\ln 2} + \frac{2\Re\{\bar{\mu}^*\mu\}}{\ln 2} - \frac{|\bar{\mu}|^2\left(1+|\mu|^2\right)}{\left(1+|\bar{\mu}|^2\right)\ln 2}, \tag{4a}$$

$$\log_2(1+\nu) \leq \log_2(1+\bar{\nu}) + \frac{\nu-\bar{\nu}}{(1+\bar{\nu})\ln 2}, \tag{4b}$$

where $\bar{u}$ and $\bar{\nu}$ are fixed points. Furthermore, according to (4a), it follows

$$\log_2\left(C+|\mu_1|^2\right) \geq \log_2\left(C+|\bar{\mu}_1|^2\right) - \frac{|\bar{\mu}_1|^2}{\ln 2} + \frac{2\Re\{\bar{\mu}_1^*\mu_1\}}{\ln 2} - \frac{|\bar{\mu}_1|^2\left(C+|\mu_1|^2\right)}{\left(C+|\bar{\mu}_1|^2\right)\ln 2}, \tag{5}$$

where $C = 1+\sum_{i=2}^{L}|\mu_i|^2$. Thus, by using (5) with respect to μ_i by fixing other μ_i from $i=2$ to $i=L$, we obtain

$$\log_2\left(1+\sum_{i=1}^{L}|\mu_i|^2\right) \geq \log_2\left(1+\sum_{i=1}^{L}|\bar{\mu}_i|^2\right) - \frac{\sum_{i=1}^{L}|\bar{\mu}_i|^2}{\ln 2} + \frac{\sum_{i=1}^{L}2\Re\{\bar{\mu}_i^*\mu_i\}}{\ln 2} - \frac{\left(\sum_{i=1}^{L}|\bar{\mu}_i|^2\right)\left(1+\sum_{i=1}^{L}|\mu_i|^2\right)}{\left(1+\sum_{i=1}^{L}|\bar{\mu}_i|^2\right)\ln 2}, \tag{6}$$

where $\{\bar{\mu}_i\}_{i=1}^{L}$ is a fixed point. [2]

Then, based on (4b) and (6), and for fixed $\{\mathbf{w}^t, \mathbf{v}^t, \mathbf{\Phi}^t\}$, we obtain a lower bound of $R_u - R_k$, which is denoted as $R_{s,k}$ and shown in (7), with the revelent variables are given in (8). Both of the two equations are shown in the next page.

With the assistance of $R_{s,k}$, we obtain an approximated problem in the t-th iteration as follows

$$\max_{\mathbf{w},\mathbf{v},\mathbf{\Phi}} F^t(\mathbf{w},\mathbf{v},\mathbf{\Phi}) \triangleq \min_k R_{s,k} \quad \text{s.t. (3b)} - \text{(3e)}. \tag{9}$$

However, (9) is not joint convex w.r.t. $\{\mathbf{w},\mathbf{v},\mathbf{\Phi}\}$ due to the product items $\mathbf{\Phi F w}$ and $\mathbf{\Phi F v}$ in a_u, b_u, a_k and b_k. Fortunately, by fixing $\{\mathbf{w},\mathbf{v}\}$ or $\mathbf{\Phi}$, (9) can be further decouple into two convex subproblems, which will be addressed in the following parts.

[2] In the t-th iteration, $\bar{\nu}$ and $\{\bar{\mu}_i\}_{i=1}^{L}$ can be valued by the obtained ν and $\{\mu_i\}_{i=1}^{L}$ in the previous iteration, i.e., we set $\bar{\nu} = \nu^{t-1}$ and $\bar{\mu}_i = \mu_i^{t-1}, \forall i = 1,\ldots,L$, in this work.

B. Optimization of $\{\mathbf{w},\mathbf{v}\}$

By conducting necessary operations and omitting the irrelevant term, we obtain the following problem w.r.t. $\{\mathbf{w},\mathbf{v}\}$ with fixed $\{\mathbf{w}^t,\mathbf{v}^t,\mathbf{\Phi}^t\}$

$$\max_{\mathbf{w},\mathbf{v}} \quad r \tag{10a}$$

$$\text{s.t. } 2\Re\left\{\mathbf{x}^H\mathbf{w}\right\} - \mathbf{w}^H\mathbf{X}_k\mathbf{w} + 2\Re\left\{\mathbf{y}_k^H\mathbf{v}\right\} - \mathbf{v}^H\mathbf{Y}_k\mathbf{v} - c_k + \frac{2\sigma_r^2\bar{\mathbf{h}}_k^H\mathbf{\Phi}^t(\mathbf{\Phi}^t)^H\bar{\mathbf{h}}_k}{\ln 2} \geq r, \forall k\in\mathcal{K}, \tag{10b}$$

$$\text{(3b), (3c), (3e)}, \tag{10c}$$

where the revelent variables are shown in (11) in the next page. Since $\mathbf{X}_k$ and $\mathbf{Y}_k$ are all positive semidefinite matrices, (10) is a QCQP and can be solved by the toolbox CVX [21].

C. Optimization of $\mathbf{\Phi}$

By using (7) and conducting necessary operations, we have the following problem w.r.t. $\mathbf{\Phi}$ with fixed $\{\mathbf{w}^t,\mathbf{v}^t,\mathbf{\Phi}^t\}$

$$\max_{\mathbf{\Phi}} \quad r \tag{12a}$$

$$\text{s.t. } -\mathrm{Tr}\left(\mathbf{\Phi Z\Phi}^H\left(\frac{a_u^t}{1+a_u^t}+\frac{1}{1+b_u^t}\right)\bar{\mathbf{h}}_u\bar{\mathbf{h}}_u^H\right) - \mathrm{Tr}\left(\mathbf{\Phi Z\Phi}^H\left(\frac{1}{1+a_k^t}+\frac{b_k^t}{1+b_k^t}\right)\bar{\mathbf{h}}_k\bar{\mathbf{h}}_k^H\right) + 2\Re\left\{\mathrm{Tr}\left(\mathbf{\Phi P}_k\right)\right\} - p_k \geq r, \forall k\in\mathcal{K}, \tag{12b}$$

$$\mathbf{g}_s^H\mathbf{\Sigma}\mathbf{g}_s + \mathrm{Tr}\left(\mathbf{\Phi Z\Phi}^H\mathbf{h}_s\mathbf{h}_s^H\right) + 2\Re\left\{\mathrm{Tr}\left(\mathbf{\Phi F\Sigma}\mathbf{g}_s\mathbf{h}_s^H\right)\right\} \leq I_{th}, \tag{12c}$$

$$\mathrm{Tr}\left(\mathbf{\Theta Z\Theta}^H\right) \leq P_r, |\phi_m| \leq \alpha_{m,\max}, \forall m. \tag{12d}$$

where the revelent variables are shown in (13) in the next page. Then, we introduce the following lemma to vectorize $\mathbf{\Phi}$ and recast (12) to a convex problem.

Lemma 2 [20]: Let $\{\mathbf{S}_1,\mathbf{S}_2\} \in \mathbb{C}^{m\times m}$. Assuming that $\mathbf{R} \in \mathbb{C}^{m\times m}$, $\mathbf{R} = \mathrm{Diag}(r_1,\ldots,r_m)$, $\mathbf{r} = \mathrm{diag}(\mathbf{R})$, we have:

$$\mathrm{Tr}\left(\mathbf{R}^H\mathbf{S}_1\mathbf{R}\mathbf{S}_2\right) = \mathbf{r}^H\left(\mathbf{S}_1\circ\mathbf{S}_2^T\right)\mathbf{r}, \mathrm{Tr}\left(\mathbf{R}\mathbf{S}_2\right) = \mathbf{r}^T\mathbf{s}_2, \tag{14}$$

where $\mathbf{s}_2 = \mathrm{diag}(\mathbf{S}_2)$. Then, by defining $\boldsymbol{\phi} = \mathrm{diag}(\mathbf{\Phi})$, we recast (13) as

$$\max_{\boldsymbol{\phi},r} \quad r \tag{15a}$$

$$\text{s.t. } 2\Re\left\{\boldsymbol{\phi}^T\mathrm{diag}(\mathbf{P}_k)\right\} - \boldsymbol{\phi}^H\mathbf{Q}_k\boldsymbol{\phi} - p_k \geq r, \forall k\in\mathcal{K}, \tag{15b}$$

$$\mathbf{g}_s^H\mathbf{\Sigma}\mathbf{g}_s + \boldsymbol{\phi}^H\left(\left(\mathbf{h}_s\mathbf{h}_s^H\right)\circ\mathbf{Z}^T\right)\boldsymbol{\phi} + 2\Re\left\{\boldsymbol{\phi}^T\circ\mathrm{diag}\left(\mathbf{F\Sigma}\mathbf{g}_s\mathbf{h}_s^H\right)\right\} \leq I_{th}, \tag{15c}$$

$$\boldsymbol{\phi}^H\left(\mathbf{I}\circ\mathbf{Z}^T\right)\boldsymbol{\phi} \leq P_r, |\phi_m| \leq \alpha_{m,\max}, \forall m, \tag{15d}$$

where $\mathbf{\Omega}_u = \left(\bar{\mathbf{h}}_u\bar{\mathbf{h}}_u^H\right)\circ\mathbf{Z}^T$, $\mathbf{\Pi}_k = \left(\bar{\mathbf{h}}_k\bar{\mathbf{h}}_k^H\right)\circ\mathbf{Z}^T$, and $\mathbf{Q}_k = \frac{a_u^t\mathbf{\Omega}_u}{1+a_u^t} + \frac{\mathbf{\Omega}_u}{1+b_u^t} + \frac{\mathbf{\Pi}_k}{1+a_k^t} + \frac{b_k^t\mathbf{\Pi}_k}{1+b_k^t}$, respectively.

It is noted that $\mathbf{Z}$ is positive semidefinite, thus $\left(\mathbf{h}_s\mathbf{h}_s^H\right)\circ\mathbf{Z}$ and $\mathbf{I}\circ\mathbf{Z}$ are positive semidefinite matrices. Besides, $\mathbf{P}_k$ is positive semidefinite, thus (15) is also a QCQP and can be solved by CVX [21].

D. Proposed AO algorithm

Combining the above steps, we obtain the whole AO approach which is summarized in Algorithm 1, where R_s^t denotes the obtained secrecy rate in the t-th iteration and κ denotes

$$R_{s,k} \triangleq \log_2\left(1+a_u^t\right) - \frac{a_u^t}{\ln 2} - \frac{a_u^t\left(1+a_u\right)}{\left(1+a_u^t\right)\ln 2} - \log_2\left(1+b_u^t\right) - \frac{b_u - b_u^t}{\left(1+b_u^t\right)\ln 2} - \log_2\left(1+a_k^t\right) - \frac{a_k - a_k^t}{\left(1+a_k^t\right)\ln 2} + \log_2\left(1+b_k^t\right) - \frac{b_k^t}{\ln 2} - \frac{b_k^t\left(1+b_k\right)}{\left(1+b_k^t\right)\ln 2} + \frac{2\Re\left\{\left(\mathbf{w}^t\right)^H \boldsymbol{\Upsilon}\mathbf{w}\right\}}{\ln 2} + \frac{2\Re\left\{\left(\mathbf{v}^t\right)^H \boldsymbol{\Delta}_k \mathbf{v}\right\}}{\ln 2} + \frac{2\sigma_r^2\Re\left\{\bar{\mathbf{h}}_u^H \boldsymbol{\Phi}\left(\boldsymbol{\Phi}^t\right)^H \bar{\mathbf{h}}_u\right\}}{\ln 2} + \frac{2\sigma_r^2\Re\left\{\bar{\mathbf{h}}_k^H \boldsymbol{\Phi}\left(\boldsymbol{\Phi}^t\right)^H \bar{\mathbf{h}}_k\right\}}{\ln 2}. \tag{7}$$

$$\begin{aligned}
&\boldsymbol{\Upsilon} = \left(\mathbf{F}^H\left(\boldsymbol{\Phi}^t\right)^H \bar{\mathbf{h}}_u + \bar{\mathbf{g}}_u\right)\left(\bar{\mathbf{g}}_u^H + \bar{\mathbf{h}}_u^H \boldsymbol{\Phi}\mathbf{F}\right), \boldsymbol{\Delta}_k = \boldsymbol{\Upsilon} + \left(\mathbf{F}^H\left(\boldsymbol{\Phi}^t\right)^H \bar{\mathbf{h}}_k + \bar{\mathbf{g}}_k\right)\left(\bar{\mathbf{g}}_k^H + \bar{\mathbf{h}}_k^H \boldsymbol{\Phi}\mathbf{F}\right), \\
&b_u = \left|\left(\bar{\mathbf{g}}_u^H + \bar{\mathbf{h}}_u^H \boldsymbol{\Phi}\mathbf{F}\right)\mathbf{v}\right|^2 + \sigma_r^2\left\|\bar{\mathbf{h}}_u^H \boldsymbol{\Phi}\right\|^2, a_u = \left|\left(\bar{\mathbf{g}}_u^H + \bar{\mathbf{h}}_u^H \boldsymbol{\Phi}\mathbf{F}\right)\mathbf{w}\right|^2 + b_u, b_k = \left|\left(\bar{\mathbf{g}}_k^H + \bar{\mathbf{h}}_k^H \boldsymbol{\Phi}\mathbf{F}\right)\mathbf{v}\right|^2 + \sigma_r^2\left\|\bar{\mathbf{h}}_k^H \boldsymbol{\Phi}\right\|^2, \\
&a_k = \left|\left(\bar{\mathbf{g}}_k^H + \bar{\mathbf{h}}_k^H \boldsymbol{\Phi}\mathbf{F}\right)\mathbf{w}\right|^2 + b_k, b_u^t = \left|\left(\bar{\mathbf{g}}_u^H + \bar{\mathbf{h}}_u^H \boldsymbol{\Phi}^t\mathbf{F}\right)\mathbf{v}^t\right|^2 + \sigma_r^2\left\|\bar{\mathbf{h}}_u^H \boldsymbol{\Phi}^t\right\|^2, a_u^t = \left|\left(\bar{\mathbf{g}}_u^H + \bar{\mathbf{h}}_u^H \boldsymbol{\Phi}^t\mathbf{F}\right)\mathbf{w}^t\right|^2 + b_u^t, \\
&b_k^t = \left|\left(\mathbf{g}_k^H + \mathbf{h}_k^H \boldsymbol{\Phi}^t\mathbf{F}\right)\mathbf{v}^t\right|^2 + \sigma_r^2\left\|\bar{\mathbf{h}}_k^H \boldsymbol{\Phi}^t\right\|^2, a_k^t = \left|\left(\bar{\mathbf{g}}_k^H + \bar{\mathbf{h}}_k^H \boldsymbol{\Phi}^t\mathbf{F}\right)\mathbf{w}^t\right|^2 + b_k^t.
\end{aligned} \tag{8}$$

$$\begin{aligned}
&\boldsymbol{\Xi} = \left(\mathbf{F}^H\left(\boldsymbol{\Phi}^t\right)^H \bar{\mathbf{h}}_u + \bar{\mathbf{g}}_u\right)\left(\bar{\mathbf{g}}_u^H + \bar{\mathbf{h}}_u^H \boldsymbol{\Phi}^t\mathbf{F}\right), \boldsymbol{\Psi}_k = \left(\mathbf{F}^H\left(\boldsymbol{\Phi}^t\right)^H \bar{\mathbf{h}}_k + \bar{\mathbf{g}}_k\right)\left(\bar{\mathbf{g}}_k^H + \bar{\mathbf{h}}_k^H \boldsymbol{\Phi}^t\mathbf{F}\right), \mathbf{x} = \frac{\boldsymbol{\Xi}\mathbf{w}^t}{\ln 2}, \\
&\mathbf{X}_k = \frac{a_u^t \boldsymbol{\Xi}}{\left(1+a_u^t\right)\ln 2} + \frac{\boldsymbol{\Psi}_k}{\left(1+a_k^t\right)\ln 2}, \mathbf{y}_k = \frac{\left(\boldsymbol{\Xi}+\boldsymbol{\Psi}_k\right)\mathbf{v}^t}{\ln 2}, \mathbf{Y}_k = \mathbf{X}_k + \frac{\boldsymbol{\Xi}}{\left(1+b_u^t\right)\ln 2} + \frac{b_k^t \boldsymbol{\Psi}_k}{\left(1+b_k^t\right)\ln 2}, \\
&c_k = \log_2\left(1+a_k^t\right) - \frac{a_k^t}{\left(1+a_k^t\right)\ln 2} - \log_2\left(1+b_k^t\right) + \frac{b_k^t}{\ln 2} + \frac{b_k^t}{\left(1+b_k^t\right)\ln 2}.
\end{aligned} \tag{11}$$

$$\begin{aligned}
&\mathbf{V} = \mathbf{v}^t\left(\mathbf{v}^t\right)^H, \boldsymbol{\Sigma} = \mathbf{w}^t\left(\mathbf{w}^t\right)^H + \mathbf{V}, \mathbf{Z} = \mathbf{F}\boldsymbol{\Sigma}\mathbf{F}^H + \sigma_r^2\mathbf{I}, \mathbf{P}_k = -\frac{a_u^t\left(\mathbf{F}\boldsymbol{\Sigma}\bar{\mathbf{g}}_u\bar{\mathbf{h}}_u^H\right)}{1+a_u^t} - \frac{\left(\mathbf{F}\mathbf{V}\bar{\mathbf{g}}_u\bar{\mathbf{h}}_u^H\right)}{1+b_u^t} - \frac{\left(\mathbf{F}\boldsymbol{\Sigma}\bar{\mathbf{g}}_k\bar{\mathbf{h}}_k^H\right)}{1+a_k^t} \\
&- \frac{b_k^t\left(\mathbf{F}\mathbf{V}\bar{\mathbf{g}}_k\bar{\mathbf{h}}_k^H\right)}{1+b_k^t} + \left(\mathbf{F}\boldsymbol{\Sigma}\left(\mathbf{F}^H\left(\boldsymbol{\Phi}^t\right)^H\bar{\mathbf{h}}_u + \bar{\mathbf{g}}_u\right)\bar{\mathbf{h}}_u^H + \mathbf{F}\mathbf{V}\left(\mathbf{F}^H\left(\boldsymbol{\Phi}^t\right)^H\bar{\mathbf{h}}_k + \bar{\mathbf{g}}_k\right)\bar{\mathbf{h}}_k^H + \sigma_r^2\left(\boldsymbol{\Phi}^t\right)^H\left(\bar{\mathbf{h}}_u\bar{\mathbf{h}}_u^H + \bar{\mathbf{h}}_k\bar{\mathbf{h}}_k^H\right)\right), \\
&p_k = c_k + \frac{\left(\mathbf{w}^t\right)^H\bar{\mathbf{g}}_k\bar{\mathbf{g}}_k^H\mathbf{w}^t}{\left(1+a_k^t\right)\ln 2} + \frac{\left(\mathbf{v}^t\right)^H\bar{\mathbf{g}}_k\bar{\mathbf{g}}_k^H\mathbf{v}^t}{\left(1+a_k^t\right)\ln 2} + \frac{b_k^t\left(\mathbf{v}^t\right)^H\bar{\mathbf{g}}_k\bar{\mathbf{g}}_k^H\mathbf{v}^t}{\left(1+b_k^t\right)\ln 2} - \frac{2\Re\left\{\left(\mathbf{v}^t\right)^H\left(\mathbf{F}^H\left(\boldsymbol{\Phi}^t\right)^H\bar{\mathbf{h}}_k + \bar{\mathbf{g}}_k\right)\bar{\mathbf{g}}_k^H\mathbf{v}^t\right\}}{\ln 2}.
\end{aligned} \tag{13}$$

the stopping threshold. In addition, for Algorithm 1, we have the following two Theorems.

Theorem 1: Algorithm 1 generates a sequence $\{\mathbf{w}^t, \mathbf{v}^t, \boldsymbol{\Phi}^t\}$ of improved points of (3), which guarantees to converge.

Proof: Please refer to Appendix A. ∎

Theorem 2: The converged solution $\{\mathbf{w}^\star, \mathbf{v}^\star, \boldsymbol{\Phi}^\star\}$ is a Karush-Kuhn-Tucker (KKT) point.

Proof: Please refer to Appendix B. ∎

Algorithm 1 The AO algorithm.

1: Initialize $\left\{\mathbf{w}^0, \mathbf{v}^0, \boldsymbol{\Phi}^0\right\}$ and set $t = 0$.
2: **repeat**
   a) Obtain $\{\mathbf{w}, \mathbf{v}\}$ via solving problem (10) with fixed $\left\{\mathbf{w}^{t-1}, \mathbf{v}^{t-1}, \boldsymbol{\Phi}^{t-1}\right\}$.
   b) Obtain $\boldsymbol{\Phi}$ via solving problem (15) with fixed $\left\{\mathbf{w}^{t-1}, \mathbf{v}^{t-1}, \boldsymbol{\Phi}^{t-1}\right\}$.
   c) $\left\{\mathbf{w}^t, \mathbf{v}^t, \boldsymbol{\Phi}^t\right\} \leftarrow \{\mathbf{w}, \mathbf{v}, \boldsymbol{\Phi}\}$.
   d) Update all the related variables.
   e) Calculate R_s^t and $t \leftarrow t+1$.
3: **until** $R_s^t - R_s^{t-1} \le \kappa$.
4: Output $\left\{\mathbf{w}^\star, \mathbf{v}^\star, \boldsymbol{\Phi}^\star\right\}$.

We now calculate the computational complexity of Algorithm 1, which is determined by the complexities of each subproblems and the number of iterations. According to [22], for problems (10) and (15), the complexities are given by $\mathcal{O}\left(2\left(K+3\right)N^2\right)$ and $\mathcal{O}\left(\left(K+3\right)M^2\right)$, respectively. Thus, the total complexity of Algorithm 1 is

$$\mathcal{C} = \mathcal{O}\left(T\left(K+3\right)\left(\max\left\{2N^2, M^2\right\}\right)\right). \tag{16}$$

with T being the number of iterations. Therefore, Algorithm 1 has the polynomial time complexity.

IV. Simulation Results

Here, we show the simulation result to verify the performance of the proposed scheme, where the BS, the RIS and the ES are deployed at $(10\text{ m}, 0\text{ m}, 10\text{ m})$, $(0\text{ m}, 50\text{ m}, 10\text{ m})$, and $(10\text{ m}, 60\text{ m}, 2\text{ m})$, respectively. We assume that there exists 3 Eves, and the MU and Eves are randomly deployed in a circle centered at $(10\text{ m}, 50\text{ m}, 2\text{ m})$ with radius 5 m. The main parameters are set as follows unless specified: $N = 4$, $M = 40$, $P_s = -10$ dBW, $P_r = 0$ dBW,[3] $I_{th} = -50$ dBW, all noise power is -80 dBm, the maximum achievable amplitude is $\alpha_{m,\max} = 10, \forall m$, and $\kappa = 10^{-3}$. The path loss is $\mathrm{PL} = 10^{-3}d^{-\alpha}$, where d is the distance and α is the loss exponent. Here, the BS to ES/MU/Eves channel is modeled as Rayleigh fading with $\alpha = 4$, and all the RIS-related links are modeled as Rician fading with $\alpha = 2.2$. More details about the channel settings are referred to [10].

Firstly, we validate the convergence behaviour of Algorithm 1 in Fig. 2, where we can find that the secrecy rate always converge within 50 iterations for different parameters, which verifies the convergence of the proposed design.

[3]It should be pointed that since the passive RIS has no transmit power consumption when comparing with the active RIS, we add this term to the transmit power budget at the BS when using the passive RIS for a fair comparison. For more details about the power consumption model about an active RIS, readers can refer to [17] and [18].

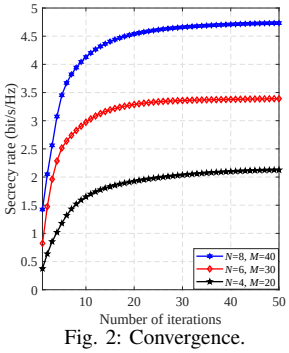

Fig. 2: Convergence.

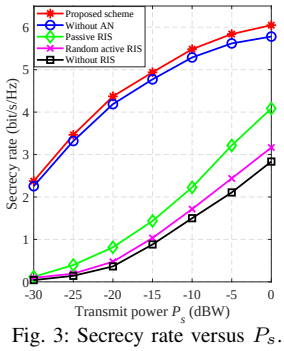

Fig. 3: Secrecy rate versus P_s.

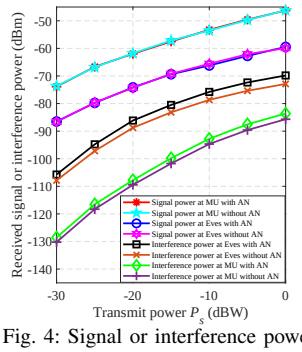

Fig. 4: Signal or interference power.

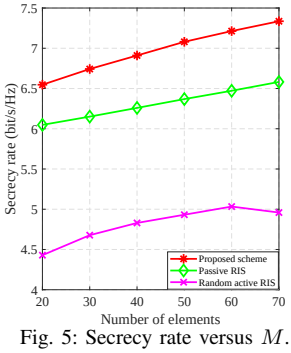

Fig. 5: Secrecy rate versus M.

Then, we investigate the secrecy rate versus P_s in Fig. 3, where we compare the proposed design with the following baselines: 1) passive RIS scenario; 2) without RIS scenario; 3) without AN design; 4) active RIS with random RC, which are labelled as "Proposed scheme", "Passive RIS", "Without RIS", "Without AN", and "Random active RIS", respectively. As we can observe, the secrecy rate obtained by all these schemes increases with P_s, and all RIS-aided schemes significantly outperform the no-RIS-aided designs. Besides, the active RIS scheme significantly outperforms the passive RIS design, mainly owing to the power amplification effect which alleviates the impact of "multiplicative fading" [17]. Thus, the received signal power at the MU is enhanced and the secrecy rate is improved. It can be observed that the increasing trends of the secrecy rate against P_s in Fig. 3 are different for the proposed scheme and the passive RIS design. This is mainly due to the fact that when P_s is relatively large when compared with P_r, the main power bottleneck of the network is P_r. Thus, the secrecy rate increases more slowly in the high P_s region. However, since passive RIS has no transmit power constraint, the secrecy rate grows more quickly in the high P_s region when using the passive RIS. Therefore, it is more beneficial to use active RIS when P_s is relatively low. In addition, since random RC cannot control the reflected signal precisely, the random RC scheme suffers obvious performance loss, even worse than the passive RIS design. This result suggests the importance of optimizing the RC properly.

Besides, from Fig. 3, we can see that the performance difference between the proposed scheme and the scheme without AN is not significant. To provide more insight to justify this observation, in Fig. 4, we show the obtained signal power/interference power at the MU/Eves either with or without AN. From Fig. 4, we observe the following facts: 1) Either with or without AN, the received signal power changes sightly at the MU/Eves; 2) The received interference power at the MU/Eves is sightly higher with AN when compared to the no AN case; 3) Either with or without AN, the signal power at the MU/Eves is always significantly higher than the interference power. Thus, we can conclude that the secrecy rate is mainly affected by the received signal power at the MU/Eves and AN has no significant effect on the system performance.

Lastly, we plot the secrecy rate versus M in Fig. 5. As we can observe, except the random RC scheme, the secrecy rate increases with M for both active and passive RIS-aided schemes due to the increased spatial degree of freedom. In addition, when given the same M, the active RIS scheme outperforms the passive-RIS scheme. In other words, we can use an active RIS with less elements to obtain the same secrecy rate when comparing with a passive RIS.

V. Conclusion

This work has studied the application of active RIS in secure CSTN. Specifically, the objective was to maximize the secrecy rate by jointly designing the BF, the AN, and the RC. By approximating the secrecy rate, an AO algorithm was developed to solve the non-convex problem via recasting each subproblem to a convex problem. Simulation results verified the superiority of the proposed active RIS scheme over other benchmarks in improving the secrecy performance.

Appendix A
Proof of Theorem 1.

It is easy to know that the following relations hold

$$\begin{aligned} &F\left(\mathbf{w},\mathbf{v},\mathbf{\Phi}\right)\geq F^t\left(\mathbf{w},\mathbf{v},\mathbf{\Phi}\right),\forall \mathbf{w},\mathbf{v},\mathbf{\Phi},\\ &F\left(\mathbf{w}^t,\mathbf{v}^t,\mathbf{\Phi}^t\right)=F^t\left(\mathbf{w}^t,\mathbf{v}^t,\mathbf{\Phi}^t\right), \end{aligned} \tag{17}$$

where $F\left(\mathbf{w}^t,\mathbf{v}^t,\mathbf{\Phi}^t\right)$ and $F^t\left(\mathbf{w}^t,\mathbf{v}^t,\mathbf{\Phi}^t\right)$ denote the corresponding objective values of (3) and (9), respectively, when $\{\mathbf{w},\mathbf{v},\mathbf{\Phi}\}\leftarrow\{\mathbf{w}^t,\mathbf{v}^t,\mathbf{\Phi}^t\}$. Therefore, we have

$$\begin{aligned} F\left(\mathbf{w}^{t+1},\mathbf{v}^{t+1},\mathbf{\Phi}^{t+1}\right)&\geq F^t\left(\mathbf{w}^{t+1},\mathbf{v}^{t+1},\mathbf{\Phi}^{t+1}\right)\\ &> F^t\left(\mathbf{w}^t,\mathbf{v}^t,\mathbf{\Phi}^t\right)=F\left(\mathbf{w}^t,\mathbf{v}^t,\mathbf{\Phi}^t\right), \end{aligned} \tag{18}$$

where the second inequality holds due to the fact that both $\left\{\mathbf{w}^{t+1},\mathbf{v}^{t+1},\mathbf{\Phi}^{t+1}\right\}$ and $\left\{\mathbf{w}^t,\mathbf{v}^t,\mathbf{\Phi}^t\right\}$ are the optimal solutions and feasible points of (3), respectively. This result means that $\left\{\mathbf{w}^{t+1},\mathbf{v}^{t+1},\mathbf{\Phi}^{t+1}\right\}$ is a better solution to (3) than $\left\{\mathbf{w}^t,\mathbf{v}^t,\mathbf{\Phi}^t\right\}$. Furthermore, due to (3b)-(3d), we know that the sequence $\left\{\mathbf{w}^t,\mathbf{v}^t,\mathbf{\Phi}^t\right\}$ is bounded. Then, according to the Cauchy's theorem [23], there exists a convergent subsequence $\left\{\mathbf{w}^{t_\gamma},\mathbf{v}^{t_\gamma},\mathbf{\Phi}^{t_\gamma}\right\}$ with a limit point $\left\{\mathbf{w}^\star,\mathbf{v}^\star,\mathbf{\Phi}^\star\right\}$, i.e.,

$$\lim_{\gamma\to+\infty}\left[F\left(\mathbf{w}^{t_\gamma},\mathbf{v}^{t_\gamma},\mathbf{\Phi}^{t_\gamma}\right)-F\left(\mathbf{w}^\star,\mathbf{v}^\star,\mathbf{\Phi}^\star\right)\right]=0. \tag{19}$$

For any t, there exists a γ such that $t_\gamma\leq t\leq t_{\gamma+1}$, thus we have

$$\begin{aligned} 0&=\lim_{\gamma\to+\infty}\left[F\left(\mathbf{w}^{t_\gamma},\mathbf{v}^{t_\gamma},\mathbf{\Phi}^{t_\gamma}\right)-F\left(\mathbf{w}^\star,\mathbf{v}^\star,\mathbf{\Phi}^\star\right)\right]\\ &\leq\lim_{t\to+\infty}\left[F\left(\mathbf{w}^{t},\mathbf{v}^{t},\mathbf{\Phi}^{t}\right)-F\left(\mathbf{w}^\star,\mathbf{v}^\star,\mathbf{\Phi}^\star\right)\right]\\ &\leq\lim_{\gamma\to+\infty}\left[F\left(\mathbf{w}^{t_{\gamma+1}},\mathbf{v}^{t_{\gamma+1}},\mathbf{\Phi}^{t_{\gamma+1}}\right)-F\left(\mathbf{w}^\star,\mathbf{v}^\star,\mathbf{\Phi}^\star\right)\right]=0, \end{aligned} \tag{20}$$

which suggests that $\lim_{t\to+\infty}F\left(\mathbf{w}^t,\mathbf{v}^t,\mathbf{\Phi}^t\right)=F\left(\mathbf{w}^\star,\mathbf{v}^\star,\mathbf{\Phi}^\star\right)$, thus completes the proof.

APPENDIX B
PROOF OF THEOREM 2.

As mentioned above, the sequence $\{\mathbf{w}^t, \mathbf{v}^t, \mathbf{\Phi}^t\}$ will converges to $\{\mathbf{w}^\star, \mathbf{v}^\star, \mathbf{\Phi}^\star\}$ as $t \to +\infty$. Next, we write the Lagrangian function of (10) as

$$\begin{aligned}
&\mathcal{L}_1\left(\mathbf{w}, \mathbf{v}, \mathbf{\Phi}^t, \{\omega_k\}_{k=1}^K, \{\lambda_i\}_{i=1}^3\right) = -r + \\
&\sum_{k=1}^{K} \omega_k \left(-2\Re\left\{\mathbf{x}^H\mathbf{w}\right\} + \mathbf{w}^H\mathbf{X}_k\mathbf{w} - 2\Re\left\{\mathbf{y}_k^H\mathbf{v}\right\}\right. \\
&\left. + \mathbf{v}^H\mathbf{Y}_k\mathbf{v} + c_k + \frac{2\sigma_r^2\bar{\mathbf{h}}_k^H\mathbf{\Phi}^t(\mathbf{\Phi}^t)^H\bar{\mathbf{h}}_k}{\ln 2} + r\right) \\
&+ \lambda_1\left(\|\mathbf{w}\|^2 + \|\mathbf{v}\|^2 - P_s\right) \\
&+ \lambda_2\left(\|\mathbf{\Phi}\mathbf{F}\mathbf{w}\|^2 + \|\mathbf{\Phi}\mathbf{F}\mathbf{v}\|^2 + \sigma_r^2\|\mathbf{\Phi}\|^2 - P_r\right) \\
&+ \lambda_3\left(\left|\tilde{\mathbf{g}}_s^H\mathbf{w}\right|^2 + \left|\tilde{\mathbf{g}}_s^H\mathbf{v}\right|^2 + \sigma_r^2\left\|\mathbf{h}_s^H\mathbf{\Phi}\right\|^2 - I_{th}\right),
\end{aligned} \tag{21}$$

where $\{\omega_k \geq 0\}_{k=1}^K$ and $\{\lambda_i \geq 0\}_{i=1}^3$ are the dual variables for (10b) and (10c), respectively. Then, when $t \to +\infty$, the partial KKT conditions for $\mathbf{w}$ and $\mathbf{v}$ are, respectively, given by $2\sum_{k=1}^K(\omega_k^\star\mathbf{X}_k\mathbf{w}^\star - \omega_k^\star\mathbf{x}) + 2\lambda_1^\star\mathbf{w}^\star + 2\lambda_2^\star\mathbf{F}^H\mathbf{\Phi}^H\mathbf{\Phi}\mathbf{F}\mathbf{w}^\star + 2\lambda_3^\star\tilde{\mathbf{g}}_s\tilde{\mathbf{g}}_s^H\mathbf{w}^\star = \mathbf{0}$, and $2\sum_{k=1}^K(\omega_k^\star\mathbf{Y}_k\mathbf{v}^\star - \omega_k^\star\mathbf{y}_k) + 2\lambda_1^\star\mathbf{v}^\star + 2\lambda_2^\star\mathbf{F}^H\mathbf{\Phi}^H\mathbf{\Phi}\mathbf{F}\mathbf{v}^\star + 2\lambda_3^\star\tilde{\mathbf{g}}_s\tilde{\mathbf{g}}_s^H\mathbf{v}^\star = \mathbf{0}$.

Similarly, the Lagrangian function of (15) is

$$\begin{aligned}
&\mathcal{L}_2\left(\mathbf{w}^t, \mathbf{v}^t, \boldsymbol{\phi}, \{\zeta_k\}_{k=1}^K, \varsigma_1, \varsigma_2, \{\tau_m\}_{k=1}^M\right) = -r + \\
&\sum_{k=1}^{K}\zeta_k\left(-2\Re\left\{\boldsymbol{\phi}^T\mathrm{diag}\left(\mathbf{P}_k\right)\right\} + \boldsymbol{\phi}^H\mathbf{Q}_k\boldsymbol{\phi} + p_k + r\right) \\
&+\varsigma_1\Big(\boldsymbol{\phi}^H\left(\left(\mathbf{h}_s\mathbf{h}_s^H\right)\circ\mathbf{Z}^T\right)\boldsymbol{\phi} + 2\Re\left\{\boldsymbol{\phi}^T\propto\mathrm{diag}\left(\mathbf{F}\mathbf{\Sigma}\mathbf{g}_s\mathbf{h}_s^H\right)\right\}\Big) \\
&+ \varsigma_1\left(\mathbf{g}_s^H\mathbf{\Sigma}\mathbf{g}_s - I_{th}\right) + \varsigma_2\left(\boldsymbol{\phi}^H\left(\mathbf{I}\circ\mathbf{Z}^T\right)\boldsymbol{\phi} - P_r\right) \\
&+ \sum_{m=1}^{M}\tau_m\left(\phi_m\phi_m^* - \alpha_{m,\max}^2\right),
\end{aligned} \tag{22}$$

where $\{\zeta_k \geq 0\}_{k=1}^K$, $\varsigma_1 \geq 0$, $\varsigma_2 \geq 0$, and $\{\tau_m \geq 0\}_{m=1}^M$ are the dual variables for (15b)-(15d), respectively. Then, the partial KKT condition for $\boldsymbol{\phi}$ is given by $2\sum_{k=1}^K\left(\zeta_k\mathrm{diag}(\mathbf{P}_k)^H + \zeta_k\mathbf{Q}_k\right) + 2\varsigma_1\left(\left(\mathbf{h}_s\mathbf{h}_s^H\right)\circ\mathbf{Z}^T\right) + 2\mathrm{diag}\left(\mathbf{F}\mathbf{\Sigma}\mathbf{g}_s\mathbf{h}_s^H\right)^H + 2\varsigma_2\left(\mathbf{I}\circ\mathbf{Z}^T\right) + 2\sum_{m=1}^M\tau_m\mathbf{E}_m = \mathbf{0}$, where $\mathbf{E}_m$ denotes an $M \times M$ matrix with the (m,m)-th element being 1 and the others being 0. Since $\{\mathbf{w}, \mathbf{v}\}$ and $\mathbf{\Phi}$ are the optimal solutions of (10) and (15), respectively, the above KKT conditions are satisfied. Hence, the converged solution $\{\mathbf{w}^\star, \mathbf{v}^\star, \mathbf{\Phi}^\star\}$ is a KKT point.

REFERENCES

[1] V. Singh and P. K. Upadhyay, "Exploiting FD/HD cooperative-NOMA in underlay cognitive hybrid satellite-terrestrial networks," *IEEE Trans. Cognitive Commun. Network.*, vol. 8, no. 1, pp. 246–262, Mar. 2022.

[2] Z. Lin *et al.*, "SLNR-based secure energy efficient beamforming in multibeam satellite systems," *IEEE Trans. Aerosp. Electron. Syst.*, early access, Jul. 2022, doi: 10.1109/TAES.2022.3190238.

[3] Z. Lin *et al.*, "Supporting IoT with rate-splitting multiple access in satellite and aerial-integrated networks," *IEEE Internet Things J.*, vol. 8, no. 14, pp. 11123–11134, Jul. 2021.

[4] H. Guo *et al.*, "A survey on space-air-ground-sea integrated network security in 6G," *IEEE Commun. Surv. Tut.*, vol. 24, no. 1, pp. 53–87, 1st Quart. 2022.

[5] K. An *et al.*, "Secure transmission in cognitive satellite terrestrial networks," *IEEE J. Sel. Areas Commun.*, vol. 34, no. 11, pp. 3025–3037, Nov. 2016.

[6] Z. Lin *et al.*, "Joint beamforming and power allocation for satellite-terrestrial integrated networks with non-orthogonal multiple access," *IEEE J. Sel. Topics Signal Process.*, vol. 13, no. 3, pp. 657–670, Jun. 2019.

[7] D. Li, "How many reflecting elements are needed for energy-and spectral-efficient intelligent reflecting surface-assisted communication," *IEEE Trans. Commun.*, vol. 70, no. 2, pp. 1320–1331, Feb. 2022.

[8] D. Li, "Ergodic capacity of intelligent reflecting surface-assisted communication systems with phase errors," *IEEE Commun. Lett.*, vol. 24, no. 8, pp. 1646–1650, Aug. 2020.

[9] Z. Chu, W. Hao, *et al.*, "Secrecy rate optimization for intelligent reflecting surface assisted MIMO system," *IEEE Trans. Inf. Forensics Security*, vol. 16, pp. 1655–1669, 2021.

[10] H. Niu, Z. Chu, *et al.*, "Weighted sum secrecy rate maximization using intelligent reflecting surface," *IEEE Trans. Commun.*, vol. 69, no. 9, pp. 6170–6184, Sep. 2021.

[11] H. Dong, C. Hua, L. Liu, and W. Xu, "Towards integrated terrestrial-satellite network via intelligent reflecting surface," in *Proc. IEEE Int. Conf. Commun. (ICC)*, Jun. 2021, pp. 1–6.

[12] B. Zhao *et al.*, "Beamforming design for IRS-assisted uplink cognitive satellite-terrestrial networks with NOMA," in *Proc. IEEE Global Conf. Commun. (GLOBECOM)*, Dec. 2021, pp. 1–6.

[13] S. Xu *et al.*, "Robust multi-user beamforming for IRS-enhanced near-space downlink communications coexisting with satellite system," *IEEE Inter. Things J.*, early access, doi: 10.1109/JIOT.2021.3112595.

[14] Z. Lin *et al.*, "Refracting RIS aided hybrid satellite-terrestrial relay networks: Joint beamforming design and optimization," *IEEE Trans. Aerosp. Electron. Syst.*, vol. 58, no. 4, pp. 3717–3724, Aug. 2022.

[15] S. Xu *et al.*, "Intelligent reflecting surface enabled secure cooperative transmission for satellite-terrestrial integrated networks," *IEEE Trans. Veh. Tech.*, vol. 70, no. 2, pp. 2007–2011, Feb. 2021.

[16] C. You and R. Zhang, "Wireless communication aided by intelligent reflecting surface: Active or passive?" *IEEE Wireless Commun. Lett.*, vol. 10, no. 12, pp. 2659–2663, Dec. 2021.

[17] R. Long, Y.-C. Liang, Y. Pei, and E. G. Larsson, "Active reconfigurable intelligent surface-aided wireless communications," *IEEE Trans. Wireless Commun.*, vol. 20, no. 8, pp. 4962–4975, Aug. 2021.

[18] K. Liu, Z. Zhang *et al.*, "Active reconfigurable intelligent surface: Fully-connected or sub-connected?" *IEEE Commun. Lett.*, vol. 26, no. 1, pp. 167–171, Jan. 2022.

[19] K. Zhi, C. Pan *et al.*, "Active RIS versus passive RIS: Which is superior with the same power budget?" *IEEE Commun. Lett.*, vol. 26, no. 5, pp. 1150–1154, May 2022.

[20] L. Dong, H.-M. Wang, and J. Bai, "Active reconfigurable intelligent surface aided secure transmission," *IEEE Commun. Lett.*, vol. 71, no. 2, pp. 2181–2186, Feb. 2022.

[21] M. Grant and S. Boyd, CVX: Matlab software for disciplined convex programming, version 2.0 beta, Sep. 2012. Available: http://cvxr.com/cvx.

[22] S. Boyd and L. Vandenberghe, *Convex Optimization.* Cambridge, U.K.: Cambridge Univ. Press, 2004.

[23] A. A. Nasir *et al.*, "Secrecy rate beamforming for multicell networks with information and energy harvesting," *IEEE Trans. Signal Process.*, vol. 65, no. 3, pp. 677–689, Feb. 2017.

[24] C. Masouros and G. Zheng, "Exploiting known interference as green signal power for downlink beamforming optimization," *IEEE Trans. Signal Process.*, vol. 63, no. 14, pp. 3628–3640, Jul. 2015.

[25] Z. Wang, L. Liu, and S. Cui, "Channel estimation for intelligent reflecting surface assisted multiuser communications: Framework, algorithms, and analysis," *IEEE Trans. Wireless Commun.*, vol. 19, no. 10, pp. 6607–6620, Oct. 2020.

[26] C. You *et al.*, "Intelligent reflecting surface with discrete phase shifts: Channel estimation and passive beamforming," *IEEE J. Sel. Areas Commun.*, vol. 38, no. 11, pp. 2604–2620, Nov. 2020.

[27] L. Wei, C. Huang, *et al.*, "Channel estimation for RIS-empowered multi-user MISO wireless communications," *IEEE Trans. Commun.*, vol. 69, no. 6, pp. 4144–4157, Jun. 2021.